Morphodynamic diversity of the world's largest rivers: Supplementary information

Description of morphodynamic model:

The simulations reported in this paper were conducted using a new numerical model of river morphodynamics, HSTAR (Hydrodynamics and Sediment Transport in Alluvial Rivers). This code solves the depth-averaged shallow water form of the Navier-Stokes equations written in conservative form. Turbulence is represented using a zero-order eddy viscosity model. Bed shear stresses are treated using a quadratic friction law, expressed in terms of a Chezy roughness coefficient (C). Secondary circulation is represented as a function of spiral flow intensity, determined using a non-equilibrium transport model (de Vriend, 1981; Deltares, 2010). Hydrodynamic equations are solved by explicit time integration using a second-order accurate (van Leer, 1979) Godunov-type finite volume scheme, based on the HLL approximate Riemann solver (Harten *et al*., 1983). Validation of the hydrodynamic model in a large sand-bed river (the Rio Paraná, Argentina) is described elsewhere (Nicholas *et al*., 2012). In the current study, the morphodynamic model is implemented using two grain size fractions. Total sand transport rates are calculated for a single size fraction (with median particle diameter, D) using the Engelund-Hansen relation (Engelund and Hansen, 1967). The validity of this capacity based approach was evaluated by calculating the adaption length scale of sediment transport following the criterion of Begnudelli *et al*. (2010). The four simulations for which $V_S/V_*<0.25$ represent a lower limit on the suitability of this approach. Sand transport direction deviates from the mean flow direction due to the effects of secondary circulation and the gravitational deflection of sediment in the direction of the local bed slope (Ikeda, 1982; Stuiksma *et al*., 1985; Talmon *et al*., 1995). The local bed slope effect is applied only to the sand fraction transported in the bedload layer. The fraction of sediment transported as bedload is determined using the approach of van Rijn (1984; equation 45). A single cohesive fine silt fraction is represented using a second-order accurate advection-diffusion transport model, with sedimentation rates determined as an inverse function of the local shear stress using the approach of Einstein and Krone (1962). This produces spatial patterns of silt sedimentation that reflect patterns of flow competence. Changes in bed elevation and grain size composition during each model time step and within each model grid cell are determined with the Exner mass balance relation, using a constant vertical layer thickness of 1m, within which sediment is assumed to be uniformly mixed. The aim of this approach is to ensure that mass is conserved for both the silt and sand fractions, rather than to keep track of the detail of floodplain stratigraphy. To speed up channel change and allow the simulation of river evolution over long time scales (centuries), hydrodynamic and morphodynamic model time steps are decoupled. This is achieved using the established approach applied elsewhere (Lesser *et al*., 2004) in which sediment fluxes (i.e. rates of erosion and deposition) in each grid cell and time step are multiplied by a constant morphological scaling factor of 200. In effect, this means that a time step of ~3 seconds in the hydrodynamic model is equivalent to ~10 minutes of real time in the context of sediment transport and channel change. All times reported here represent real time that has been scaled in this way.

Grid cells are defined as either active channel bed or vegetated floodplain (including islands). Active channel cells are converted to floodplain cells when the maximum depth of inundation experienced over a specified time period (T_{veg}) does not exceed a given threshold depth (H_{cr}). Low T_{veg} and high H_{cr} values promote rapid vegetation colonization and floodplain development. Floodplain cells are characterised by higher roughness (a low, constant Chezy value). Vertical erosion of floodplain cells occurs only when a threshold velocity (V_{cr}) is exceeded allowing vegetation removal. Floodplain reworking occurs predominantly by lateral bank erosion. Bank erosion rates are calculated as the product of the near bank sediment transport rate parallel to the bank line, the local bank slope and a dimensionless proportionality constant representing bank erodibility (E). To prevent diffusion of topography and maintain distinct channel bank lines, bank erosion does not lead to a reduction in bank height. Instead, the volume of material removed from floodplain cells by bank erosion is recorded, and floodplain cells are converted to channel cells at the level of the channel bed once sufficient material has been removed. This representation of floodplain development and bank erosion aims to capture the first order controls on channel evolution, and is simple in order to avoid over-parameterisation of processes.

Simulations were carried out in a domain 50 km long by 16 km wide composed of 625 x 400 cells, each measuring 80 m long by 40 m wide. This cell aspect ratio provides the optimal balance between model efficiency and resolution. Additional model runs (not reported here) were conducted for a subset of simulations using different cell sizes (including 60 m by 30 m and 60 m by 60 m) to confirm that cell size and aspect ratio do not affect model results substantially. All simulations used the same initial conditions (a straight channel, 2.4 km wide, having a constant slope (S) with small (±0.1 m) white noise elevation perturbations). Inflow conditions consisted of hydrographs with a minimum discharge of 10,000 m^3s^{-1} and peak discharges that varied from 15,000 m^3s^{-1} to 30,000 m^3s^{-1} between individual floods (see Fig. DR1). A sequence of floods with varying peak discharge were generated and applied in all simulations. Sand supply rates at the inlet to the model domain were assumed to be at capacity. Silt concentrations at the inlet were held constant throughout simulations (i.e. they did not vary over the course of hydrographs). In order to introduce an upstream perturbation at the domain inlet, to encourage the development of a non-symmetrical channel, the inlet section shape was represented as a laterally inclined plane that tipped back and forth with a periodicity of 40 years. This introduces an effect equivalent to the slow migration of lateral bars though the domain inlet. Results reported here are for a total of 45 simulations. Model parameters with well documented values were varied across the range appropriate for large sand-bed rivers: S = 0.00005 m m^{-1} to 0.0002 m m^{-1}; D = 0.2 mm to 0.5 mm; C = 40 to 55 $m^{1/2}s^{-1}$. Other parameter values were varied to yield rates of bank erosion and vegetation establishment consistent with natural channels: $T_{veg} \leq 10$ years; $H_{cr} = 0.1$ m to 0.3 m; $E = 3$ to 10 for the majority (44) of simulations. Full details on model parameter values and boundary conditions for individual simulations are listed in Table DR2 below.

Quantitative analysis:

Model results are deemed to be realistic based on the consistency between simulated and observed channel width:depth ratios and degree of branching (see Tables DR1 and DR2), and because modeled bar geometries, scour pool depths, and rates of bank erosion and bar migration lie within the range of observations for large sand-bed rivers (see Table DR3). The influence on simulated channel morphology of rate of floodplain development, bank erodibility and bed sediment mobility was evaluated using the Mann-Whitney U test. The role of floodplain development rate was evaluated by comparing simulations for which vegetation colonization was rapid ($T_{veg} = 6$ years, $H_{cr} = 0.3$ m) with simulations for which colonization was slow ($T_{veg} = 10$ years, $H_{cr} = 0.1$ m), but was found to have no significant effect on morphology. Channel width and number of channel branches were found to be significantly different at the 99% level for simulations conducted using low bank erodibility ($E = 3$) compared to those conducted using high bank erodibility ($E = 10$). Channel width:depth ratio and number of channel branches were found to be significantly different at the 99% level for simulations with low bed sediment mobility ($V_S/V_* > 0.6$) compared to those with high bed sediment mobility ($V_S/V_* \leq 0.6$). The role of bed sediment mobility in controlling channel width:depth ratio and number of channel branches was also evaluated using the Spearman's rank correlation coefficient (r^2 values are given in Fig. 4 and Fig. DR2). Figure DR2 quantifies bed sediment mobility using a metric that is independent of channel morphology (i.e. unrelated to width or depth).

Supplementary Movies:

Supplementary movies DR1 and DR2 show examples of simulated channel evolution for two contrasting model setups (runs 21 and 6) that promote, respectively, channel-dominated and bar-island-dominated behaviour. In both movies, the river morphology is shown for low flow conditions only, although channel evolution is a response to a sequence of flow hydrographs. High flow conditions are not shown in the movies to aid clarity, because variation in river discharge makes visualisation of channel change more difficult.

Table DR1: Morphological characteristics of large alluvial rivers

River (gauge or location)	Q_{bf}	D	S_C	σ	N	W	H	$<W>/H$	V_S/V_*
Amazon (Jatarana)	161,330	0.25	0.000021	1.16	2.28	4800	27.81	75.69	0.464
Solimões - Amazon (Manacapuru)	120,000	0.25	0.000018	1.1	1.88	4200	26.28	85.02	0.515
Solimões - Amazon (Itapeua)	90,000	0.2	0.000016	1.2	2.1	3500	25.47	65.43	0.411
Solimões (Teresina)	60,000	0.3	0.000038	1.21	1.7	2200	19.86	65.17	0.510
Solimões (Santo Antonio do Iça)	70,000	0.3	0.000034	1.5	1.76	2600	20.43	72.31	0.532
Araguaia (Luis Alves)	3,700	0.3	0.000100	1.05	1.4	525	5.84	64.27	0.580
Araguaia (Aruana)	3,200	0.4	0.000150	1.23	1.5	475	4.95	64.02	0.695
Araguaia (São Felix)	6,000	0.3	0.000098	1.46	1.65	925	5.56	100.86	0.601
Fly (Kuambit)	3,018	0.2	0.000050	1.67	1.03	200	12.21	15.90	0.336
Iça (Ipiranga)	10,213	0.3	0.000082	1.84	1.14	750	9.67	68.03	0.498
Japurá (Acanauí)	21,000	0.4	0.000036	1.05	2.54	2150	10.20	83.02	0.988
Japurá (Vila Bittencourt)	20,000	0.4	0.000041	1.05	2.1	2000	9.92	96.03	0.939
Juruá (Eurinepê)	3,000	0.3	0.000072	2.31	1	200	10.77	18.57	0.503
Juruá (Santos Dumont)	7,700	0.3	0.000080	2.3	1	350	13.43	26.07	0.428
Madeira (Abunã)	25,000	0.3	0.000060	1.15	1.02	825	18.29	44.21	0.423
Madeira (Porto Velho)	30,000	0.2	0.000043	1.3	1.2	1100	19.06	48.11	0.290
Madeira (Manicoré)	42,000	0.2	0.000041	1.25	1.04	1300	21.68	57.67	0.278
Madeira (Fazenda Vista Alegre)	57,000	0.2	0.000057	1.19	1.34	1850	18.82	73.37	0.253
Mamoré (Guajará-Mirim)	14,700	0.3	0.000090	1.45	1.06	650	13.15	46.64	0.407
Negro (Mariuá)	29,000	0.45	0.000045	1.08	4.38	5200	6.51	182.24	1.231
Orinoco (Musinacio)	64,600	0.4	0.000060	1.10	1.85	3200	13.95	123.96	0.654
Paraguay (Porto Murtinho)	3,333	0.3	0.000040	1.39	1.16	460	8.07	49.16	0.780
Paraná (Corrientes)	27,330	0.4	0.000049	1.25	2.28	2650	9.54	121.83	0.876
Paraná (Curtiembre)	20,500	0.3	0.000048	1.2	2.26	2300	8.72	116.77	0.685
Paraná (Villa Urquiza)	17,140	0.3	0.000044	1.19	1.54	2000	8.74	148.59	0.715
Purus (Beaba. Cariuacanga)	16,711	0.3	0.000032	1.57	1	700	19.24	36.38	0.565
Purus (Valparaíso)	6,000	0.3	0.000093	1.71	1	270	12.85	21.00	0.405
Purus (Lábrea)	10,550	0.3	0.000065	2.08	1	425	15.59	27.25	0.440
Upper Paraná (Porto Rico)	12,300	0.3	0.000110	1.05	2.98	2050	5.08	135.48	0.593
Jamuna (Bahadurabad)	60,000	0.25	0.000068	1.1	-	7500	7.22	-	0.506

Q_{bf} is bankfull discharge (m^3s^{-1}), approximated by the mean annual discharge in the case of the Negro, D is bed sediment diameter (mm), S_C is channel gradient, σ is sinuosity, N is the average number of channel branches at a cross-section, W is channel width (m) excluding islands, $<W>$ is the average width of individual channel branches, H is mean bankfull channel depth (m), V_S is the particle settling velocity ($m\,s^{-1}$), and V_* is mean shear velocity ($m\,s^{-1}$). Values of Q_{bf}, D, and S_C were obtained from published literature (Latrubesse and Franzinelli, 2005; Latrubesse, 2008). Values of W, σ, and N were obtained by analysis of imagery. A 50-100 km length of channel was selected from Landsat images (courtesy of the United States Geological Survey). In the case of the Rio Araguaia, Google Earth images were also examined. Sinuosity values were determined for the dominant channel branch in each river (or calculated as the average of values for individual branches of similar size, where no single branch is clearly dominant), and from values reported by Kleinhans and van den Berg (2011). Values of N were determined by counting channels at cross-sections spaced at 1 km intervals throughout each reach. Values of W were determined as the average width at these sections. For the majority of rivers in the dataset, channel branches are separated by vegetated islands that are emergent across a wide range of flows. In such cases, the number of branches is relatively insensitive to river stage. The Jamuna River is a significant exception to this and N is difficult to characterize for this river using a single value. Consequently, N is not shown in Table DR1 for this river, although it should be noted, as discussed in the main text, that branch numbers are high (typically 4-6 and >10 at some sections). Values of $<W>$ were calculated as $<W> = W / N$, hence $<W>$ was not calculated for the Jamuna. Values of H were calculated by combining the flow continuity equation with a Chezy roughness law to yield $H = (Q_{bf} / (W\, C\, S_C^{1/2}))^{2/3}$, where C is the Chezy roughness coefficient, which was assigned a constant value of 50 $m^{1/2}s^{-1}$. Values of V_* were calculated as $V_* = (g\, H\, S_C)^{1/2}$, where g is acceleration due to gravity.

Table DR2: Parameter values and morphological characteristics for numerical model runs

Run	S	C	D	L	E	T_{veg}	H_{cr}	N	W/H	V_S/V_*
1	0.00005	55	0.2	150	10	10	0.1	2.24	102.35	0.509
2	0.00005	55	0.4	150	10	10	0.1	2.77	152.92	1.071
3	0.00005	55	0.2	150	3	10	0.1	1.63	81.63	0.474
4	0.00005	55	0.4	150	3	10	0.1	2.42	186.28	1.089
5	0.00005	55	0.2	450	10	6	0.3	2.53	104.94	0.509
6	0.00005	55	0.4	450	10	6	0.3	2.59	155.41	1.071
7	0.00005	55	0.2	450	3	6	0.3	1.79	68.31	0.457
8	0.00005	55	0.4	450	3	6	0.3	2.36	174.24	1.089
9	0.0001	55	0.2	150	10	10	0.1	1.65	81.45	0.351
10	0.0001	55	0.4	150	10	10	0.1	2.71	105.58	0.878
11	0.0001	55	0.2	150	3	10	0.1	1.62	73.69	0.334
12	0.0001	55	0.4	150	3	10	0.1	2.14	110.69	0.790
13	0.0001	55	0.2	450	10	6	0.3	2.08	81.39	0.316
14	0.0001	55	0.4	450	10	6	0.3	2.29	99.55	0.974
15	0.0001	55	0.2	450	3	6	0.3	1.43	75.2	0.316
16	0.0001	55	0.4	450	3	6	0.3	1.95	98.75	0.755
17	0.0001	40	0.2	150	10	10	0.1	2.08	60.75	0.332
18	0.0001	40	0.4	150	10	10	0.1	3.43	95.79	0.868
19	0.0001	40	0.2	150	3	10	0.1	1.88	54.65	0.346
20	0.0001	40	0.4	150	3	10	0.1	2.14	75.09	0.690
21	0.0001	40	0.2	450	10	6	0.3	2.56	65.64	0.332
22	0.0001	40	0.4	450	10	6	0.3	3	91.83	0.881
23	0.0001	40	0.2	450	3	6	0.3	1.96	51.78	0.358
24	0.0001	40	0.4	450	3	6	0.3	2.37	84.99	0.715
25	0.0002	40	0.2	150	10	10	0.1	1.78	53.29	0.230
26	0.0002	40	0.4	150	10	10	0.1	2.89	78.35	0.690
27	0.0002	40	0.2	150	3	10	0.1	1.55	59.07	0.230

28	0.0002	40	0.4	150	3	10	0.1	2.29	71.75	0.575
29	0.0002	40	0.2	450	10	6	0.3	2.13	58.15	0.217
30	0.0002	40	0.4	450	10	6	0.3	2.81	79.99	0.626
31	0.0002	40	0.2	450	3	6	0.3	1.59	58.08	0.230
32	0.0002	40	0.4	450	3	6	0.3	2.74	77.33	0.600
33	0.00005	55	0.3	450	10	6	0.3	2.65	125.42	0.808
34	0.0001	55	0.3	450	10	6	0.3	2.45	95.76	0.650
35	0.0001	40	0.3	450	10	6	0.3	2.56	82.57	0.613
36	0.0002	40	0.3	450	10	6	0.3	2.58	69.8	0.460
37	0.00005	55	0.3	450	3	6	0.3	2.53	132.33	0.755
38	0.0001	55	0.3	450	3	6	0.3	1.9	92.96	0.579
39	0.0001	40	0.3	450	3	6	0.3	1.74	63.17	0.562
40	0.0002	40	0.3	450	3	6	0.3	2.39	68.8	0.409
41	0.00005	55	0.5	150	10	6	0.3	2.73	120.19	1.075
42	0.00005	55	0.5	150	10	10	0.1	2.66	156.11	1.099
43	0.00005	55	0.5	450	3	6	0.3	2.3	147.1	1.071
44	0.00005	55	0.5	450	3	10	0.1	2.3	128.37	1.106
45	0.0001	40	0.25	150	10	50	0.01	2.26	79.73	0.511

S is channel slope, *C* is Chezy roughness ($m^{1/2}s^{-1}$), *D* is bed sediment diameter (mm), *L* is inlet silt concentration (mg l^{-1}), *E* is dimensionless bank erodibility, T_{veg} is time (years) that flow depths must not exceed H_{cr} (m) for channel cells to be converted to floodplain, *N* is the average number of channel branches at a cross-section, *W/H* is the channel width:depth ratio, and V_S/V_* is the ratio of the particle fall velocity to the mean shear velocity. Channel characteristics (*N*, *W/H* and V_S/V_*) reported in Table DR2 represent the average values throughout the model domain over the final 20 years of model simulations.

Table DR3: Morphodynamic characteristics of modeled and natural rivers

Characteristic	**Modeled rivers**	**Natural rivers**
Bar length/width	10th percentile of bar distribution: 1.45 – 1.75 50th percentile of bar distribution: 2.90 – 3.20 90th percentile of bar distribution: 5.20 – 8.00	10th percentile of bar distribution: 1.26[1], 1.31[2] 50th percentile of bar distribution: 2.39[1], 2.67[2] 90th percentile of bar distribution: 3.65[1], 4.55[2]
Island length/width	10th percentile of island distribution: 1.65 – 2.50 50th percentile of island distribution: 3.00 – 3.90 90th percentile of island distribution: 6.20 – 8.00	10th percentile of island distribution: 1.94[1], 2.79[3] 50th percentile of island distribution: 3.35[1], 4.26[3] 90th percentile of island distribution: 5.48[1], 7.16[3]
Maximum scour pool depth	25 – 35 m	Rio Paraná: 20 – 26 m Jamuna River: Up to 40 m
Compound bar migration rate	Up to 300 m y^{-1}	Rio Paraná: Up to 200 m y^{-1} Jamuna River: Up to 3 km y^{-1}
Bank erosion rate	Average rates: 3.5 – 38 m y^{-1} Maximum rates: 120 m y^{-1}	Rio Paraná: In zones of maximum erosion: 21 – 100 m y^{-1} Jamuna River: 50 m y^{-1} on average Maximum local rate 1 km y^{-1}

Bar and island lengths and widths for natural rivers were determined from satellite imagery for the [1]Rio Paraná, [2]Jamuna River, and [3]Rio Japurá. Bar length was determined as the longest straight line that could be drawn on the bar. Bar width was then determined as the longest line on the bar surface perpendicular to the long axis (along which bar length is measured). Islands and bars were distinguished in this analysis based on the absence (for bars) or presence (for islands) of vegetation. Equivalent definitions were used for modeled rivers. A range of values are shown for modeled bar and island length:width ratios reflecting variations between simulations. Compound bar migration rates were measured for the Rio Paraná using repeat satellite imagery. Bank erosion rates for the Rio Paraná are given by Ramonell *et al*. (2002). Scour pool depths for the Rio Paraná are given by Ramonell *et al*. (2002) and Nicholas *et al*. (2012). Bar migration rates, bank erosion rates and scour pool depths for the Jamuna are given by Ashworth and Lewin (2012).

Figure Captions:

Figure DR1: Flow conditions used in all model simulations. These consist of a series of hydrographs with peak discharges that vary between c. 15,000 m^3s^{-1} and 30,000 m^3s^{-1}.

Figure DR2: Relationship between bed sediment mobility and channel width:depth ratio in natural and simulated rivers. Sediment mobility is expressed here as the ratio of grain diameter (D) to the square root of valley gradient (S). This provides an index of sediment mobility that is independent of channel depth, and hence width:depth ratio. Model results represent average values over the final 20 years of each simulation, and are divided into two subsets with strong banks (E = 3) and weak banks (E = 10). Data for natural rivers (crosses) are listed in Table DR1. All correlations are significant at the 99% level or better.

References:

Ashworth, P.J., and Lewin, J. 2012. How do big rivers come to be different? *Earth Science Reviews* 114, 84-107.

Begnudelli, L., Valiani, A., and Sanders, B.F. 2010. A balanced treatment of secondary currents, turbulence and dispersion in a depth-integrated hydrodynamic and bed deformation model for channel bends. *Advances in Water Resources* 33, 17-33.

Deltares. 2010. Delft3D-FLOW user manual, version 3.14, Deltares.

De Vriend, H.J. 1981. Steady flow in shallow channel bends. Communications on Hydraulics, 81-3, Delft University of Technology, Delft, The Netherlands.

Einstein, H.A., and Krone, R.B. 1962. Experiments to determine modes of cohesive sediment transport in salt water. *Journal of Geophysical Research* 17, 1463-1464.

Engelund, F. & Hansen, E. 1967. A monograph on Sediment Transport in Alluvial Streams. Teknisk Forlag, Copenhagen.

Harten, A., Lax, P.D. and van Leer, B. 1983. On upstream differencing and Godunov-type schemes for hyperbolic conservation laws. *SIAM Reviews* 25, 35-6.

Ikeda, S. 1982. Lateral bed load transport on side slopes. Journal of the Hydraulics Division, ASCE, v 108, 1369-1373.

Kleinhans, M.G. and van den Berg, J.H. 2011. River channel and bar patterns explained and predicted by an empirical and physics-based method. *Earth Surface Processes and Landforms* 36, 721-738.

Latrubesse, E.M. 2008. Patterns of anabranching channels: The ultimate end-member adjustment of mega rivers. *Geomorphology* 101, 130-145.

Latrubesse, E. M. and Franzinelli, E. 2005. The late Quaternary evolution of the Negro River, Amazon, Brazil: Implications for island and floodplain formation in large anabranching tropical systems. *Geomorphology* 70, 372– 397.

Lesser, G.R., Roelvink, J.A., van Kester, J.A.T.M. and Stelling, G.S. 2004. Development and validation of a three-dimensional morphological model. Coastal Engineering 51, 883-915.

Nicholas, A.P., Sandbach, S.D., Ashworth, P.J., Amsler, M.L., Best, J.L., Hardy, R.J., Lane, S.N., Orfeo, O., Parsons, D.R., Reesink, A.J.H., Sambrook Smith, G.H. and Szupiany, R.N. 2012. Modelling hydrodynamics in the Rio Paraná, Argentina: an evaluation and inter-comparison of reduced-complexity and physics based models applied to a large sand-bed river. *Geomorphology* 169-170, 192-211.

Ramonell, C.G., Amsler, M.L., and Toniolo, H. 2002. Shifting modes of the Parana River thalweg in its middle/lower reach. *Zeitschrift fur Geomorphologie N.F.* 129, 129-142.

Struiksma, N., Olesen, K., Flokstra, C. and De Vriend, H. 1985. Bed deformation in curved alluvial channels. *Journal of Hydraulic Research* 23, 57–79.

Talmon, A., Struiksma, N. and van Mierlo, M. 1995. Laboratory measurements of the direction of sediment transport on transverse alluvial bed slopes. *Journal of Hydraulic Research* 33, 495–517.

van Leer, B. 1979. Towards the ultimate conservation difference scheme. V.A. second-order sequel to Godunov's method. *Journal of Computational Physics* 32, 101-136.

van Rijn, L.C. 1984. Sediment transport, Part II: Suspended load transport. *Journal of Hydraulic Engineering* 110, 1613-1641.

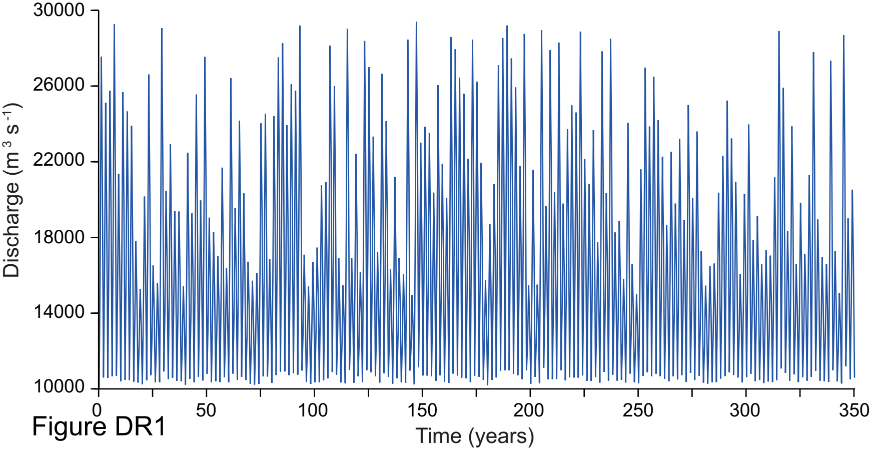
30000
26000
22000
18000
14000
10000
Discharge (m 3 s -1)
0
50
100
150
200
250
300
350
Time (years)

Figure DR1

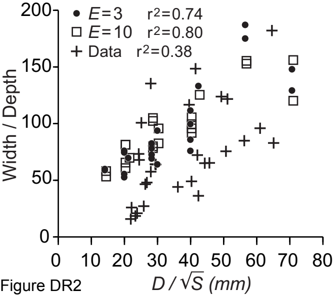

E=3 r2=0.74
E=10 r2=0.80
Data r2=0.38
Width / Depth
200
150
100
50
0
0
10
20
30
40
50
60
70
80
D / √S (mm)

Figure DR2